ChemPubSoc Europe

DOI: 10.1002/cctc.201700248

CHEMCATCHEM Full Papers

# Boron Nitride-supported Sub-nanometer $Pd_6$ Clusters for Formic Acid Decomposition: A DFT Study

Roberto Schimmenti,[a] Remedios Cortese,[a] Dario Duca,*[a] and Manos Mavrikakis*[b]

A periodic, self-consistent planewave DFT study was carried out to explore the potential use of $Pd_6$ clusters supported on a boron nitride sheet as a catalyst for the selective decomposition of formic acid (HCOOH) to $CO_2$ and $H_2$. The competition between formate (HCOO) and carboxyl (COOH) paths on catalytic sites, with different proximities to the support, was studied. Based on energetics alone, the reaction may mainly follow the HCOO route. Slightly lower activation energies were found at the lateral sites of the cluster as compared to top face sites. This is particularly true for the bidentate to monodentate HCOO conversion. Through comparison of results with similar studies on HCOOH decomposition on extended Pd surfaces, it was demonstrated that the existence of undercoordinated sites in the sub-nanometer cluster could play a key role in preferentially stabilizing HCOO over COOH, which is a common CO precursor in this reaction. A hydrogen spillover mechanism was also investigated; migration toward the boron nitride support is not favorable, at least in the early stages of the reaction. However, hydrogen diffusion on the cluster has low barriers compared to those involved in formic acid decomposition.

## Introduction

The transition toward a hydrogen-based fuel economy is intimately connected with the optimization of sustainable hydrogen production and transportation technologies. Formic acid (HCOOH) has been proposed as a promising hydrogen carrier, being nontoxic and obtainable from the upgrading of fuels and chemicals, such as levulinic acid production[1] and, to a lesser extent, from aqueous phase reforming of polyalcohols.[2] HCOOH decomposition can occur following two main paths: dehydrogenation, involving the production of formate (HCOO) or carboxyl (COOH) intermediates, or dehydration, leading to carbon monoxide and water. The latter route leads to partial poisoning of catalytic metal active sites by CO, and thus is not desirable for $H_2$ production purposes. Both paths may involve the production of formate (HCOO) or carboxyl (COOH) intermediates.

To use HCOOH as a fuel in direct formic acid fuel cells (DFAFCs) a high selectivity toward $H_2$ is required. Indeed, platinum and palladium, the most active catalysts for formic acid decomposition and typical DFAFCs anode electrocatalysts, suffer considerably from CO poisoning. Hence, different experimental and computational studies, aimed at understanding the reaction mechanism and improving the catalyst selectivity of HCOOH decomposition, have been carried out.[3–5] For example, Herron et al. have concluded through periodic DFT calculations that Ni(111), Ru(0001), Pd(100), Pt(100), and other transition-metal surfaces, could be considerably poisoned by CO when HCOOH decomposes via a COOH–mediated pathway.[6] These results are in accord with a number of experimental studies,[7–9] which place Pd(111)[10] and Ni(111)[11] on a list of CO selective surfaces. Despite a plethora of studies on HCOOH decomposition on transition-metal surfaces, the reaction mechanism is still unsettled. Importantly, little attention has been devoted to HCOOH decomposition on sub-nanometer catalysts, which have demonstrated peculiar activity and selectivity in various reactions, such as the oxidative dehydrogenation of propane and propylene epoxidation.[12] Sub-nanometer-sized clusters for HCOOH decomposition could offer a new strategy for achieving high selectivity to $H_2$. On extended surfaces, it has been shown that site coordination significantly affects HCOOH dehydrogenation.[6] Thus, highly undercoordinated sites present in sub-nanometer clusters may exhibit unexpected activity and/or selectivity. Although computational approaches are well suited for this analysis, it has been demonstrated that these catalytic systems cannot be realistically modeled without taking into account support effects.[13] In this spirit, it is appropriate to focus on emerging catalyst supports such as boron nitride based materials, which besides possessing high thermal, mechanical, and chemical resistance,[14–16] have also been recently investigated as hydrogen storage platforms[17,18] and in nanocatalysis.[19,20]

In this work, a periodic DFT study of HCOOH decomposition on a hexagonal boron nitride (*h*-BN) supported $Pd_6$ sub-nanometer clusters is presented. Particular emphasis is placed on

[a] R. Schimmenti, Dr. R. Cortese, Prof. D. Duca
Dipartimento di Fisica e Chimica
Università degli Studi di Palermo
Viale delle Scienze Ed. 17, I-90128, Palermo (Italy)
E-mail: dario.duca@unipa.it

[b] Prof. M. Mavrikakis
Department of Chemical and Biological Engineering
University of Wisconsin-Madison
Madison, Wisconsin 53706 (USA)
E-mail: emavrikakis@wisc.edu

The ORCID identification number(s) for the author(s) of this article can be found under https://doi.org/10.1002/cctc.201700248.

This publication is part of a Special Issue on "Catalysis for New Energy Technology".



© 2017 Wiley-VCH Verlag GmbH & Co. KGaA, Weinheim

reaction energetics of the HCOO- and COOH–mediated paths while considering two types of active sites having different proximities to the BN support. Further, we also present insights into possible hydrogen diffusion mechanisms to address the feasibility of hydrogen spillover from the Pd cluster to the *h*-BN support.

## Results

### $Pd_6$/*h*-BN interaction

The optimized structure of the *h*-BN supported $Pd_6$ cluster is reported in Figure 1. $Pd_6$ shows a triple atop adsorption mode, in which each of the Pd atoms interacting with the BN surface is on top of a nitrogen atom; with a Pd–N bond distance of 2.31 Å. A slightly larger average bond distance of 2.45 Å was previously determined for the same cluster adsorbed on a (12,12) armchair single-walled boron nitride nanotube (BNNT), treated at the CAM-B3LYP level of theory.[21] While $Pd_6$ in vacuo exists in an octahedral geometry, with an average Pd–Pd bond length of 2.65 Å, some distortion occurs upon adsorption on the *h*-BN support, which leads to an increased average bond distance of 2.68 Å. Indeed, owing to the interaction with the N atoms of the support, the distance between the Pd atoms lying nearest to the surface is increased, reaching a maximum of 2.73 Å. We calculated the adsorption energy of the cluster to be $-171.2\ kJ\,mol^{-1}$. A direct comparison of this value with previous reports is quite difficult owing to the relative lack of studies on similar systems at the same level of theory. As an example, on the above-mentioned BNNT a much lower adsorption energy of $-85.0\ kJ\,mol^{-1}$ was found, but this difference may be due to the different nature of systems treated as well as the computational methods employed.

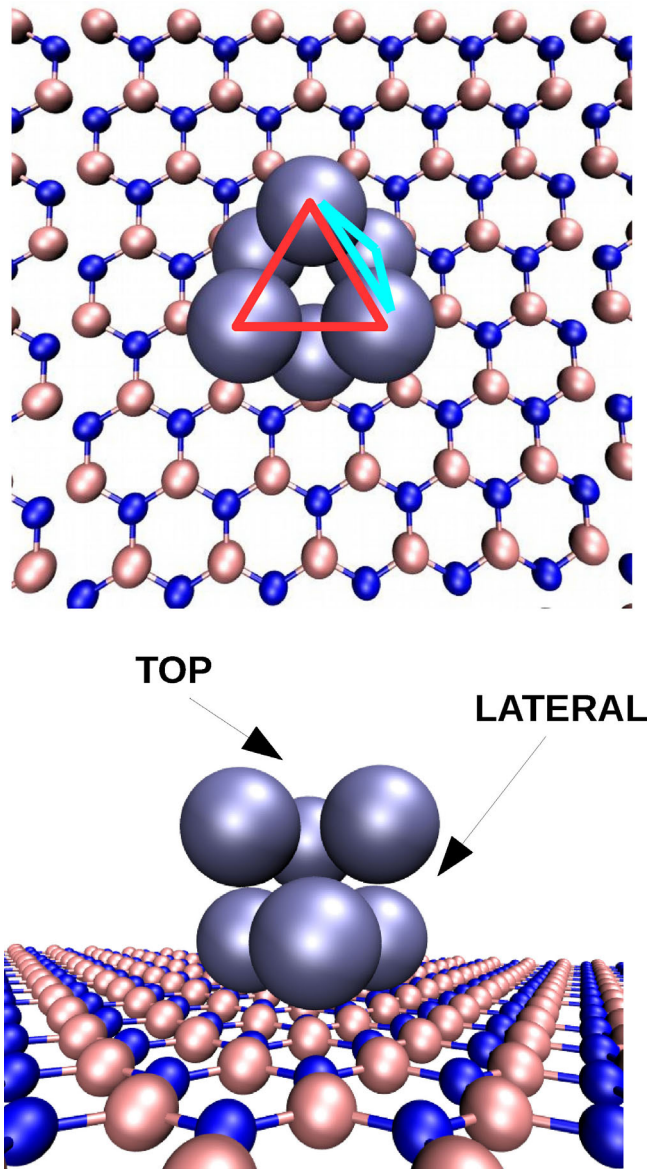


**Figure 1.** Optimized structure of the *h*-BN supported $Pd_6$ cluster. The upper panel gives a top view of the cluster. The red triangle indicates the "top" face of the cluster while the cyan triangle, the "lateral" face. These two faces are indicated in the bottom panel, which shows the front view of the structure. B, N, and Pd atoms are represented by bronze, blue and silver spheres, respectively.

Still, it can be informative to compare our obtained adsorption energy with those of other studies on selected sub-nanometer Pd clusters on typical catalytic supports. Indeed, one of the conclusions obtained in most experimental studies dealing with boron nitride based supports is that these supports should interact weaker with noble metal nanoparticles compared to other supports, such as carbon nanotubes (CNTs) and $\gamma$-$Al_2O_3$.[22] Our value is well below that previously calculated by Kacprzak et al.[23] for $Pd_9$ on $\gamma$-$Al_2O_3$, who found an adsorption energy of $-318.0\ kJ\,mol^{-1}$, or by Duca et al.[24] for the same cluster on a CNT, who found an adsorption energy of $-227.0\ kJ\,mol^{-1}$.

The electronic properties of adsorbed $Pd_6$ were studied by means of projected density of states (pDOS) calculations, as shown in Figure 2. The strong interaction between the cluster and the support can be ascribed to efficient overlap between the Pd 4d and N 2p states located right under the Fermi level. As a consequence of this interaction, upon adsorption of $Pd_6$, an overall broadening of the sharp peaks localized between −4 and −2 eV can be seen in Figure 2C.

Spin magnetic moment and Bader charge analysis are useful tools for the characterization of the properties of supported metal clusters. Here the *h*-BN supported $Pd_6$ has a total spin magnetic moment of 2.0 $\mu_B$, which is the same as that of $Pd_6$ in vacuo. Bader charge analysis indicates negligible charge transfer between the cluster and the support. It is interesting to compare this latter result with that of Prestianni et al.[25] regarding the interaction of a $Pd_{30}$ cluster on a BNNT surface. They report a negative charge transfer from the support to the $Pd_{30}$ cluster. This means that the amount of charge transfer may be related to both the size of the metal cluster and the intrinsic curvature of the support.

### HCOOH adsorption

We evaluated the stability of different HCOOH coordination modes on the supported $Pd_6$ cluster in terms of their


© 2017 Wiley-VCH Verlag GmbH & Co. KGaA, Weinheim

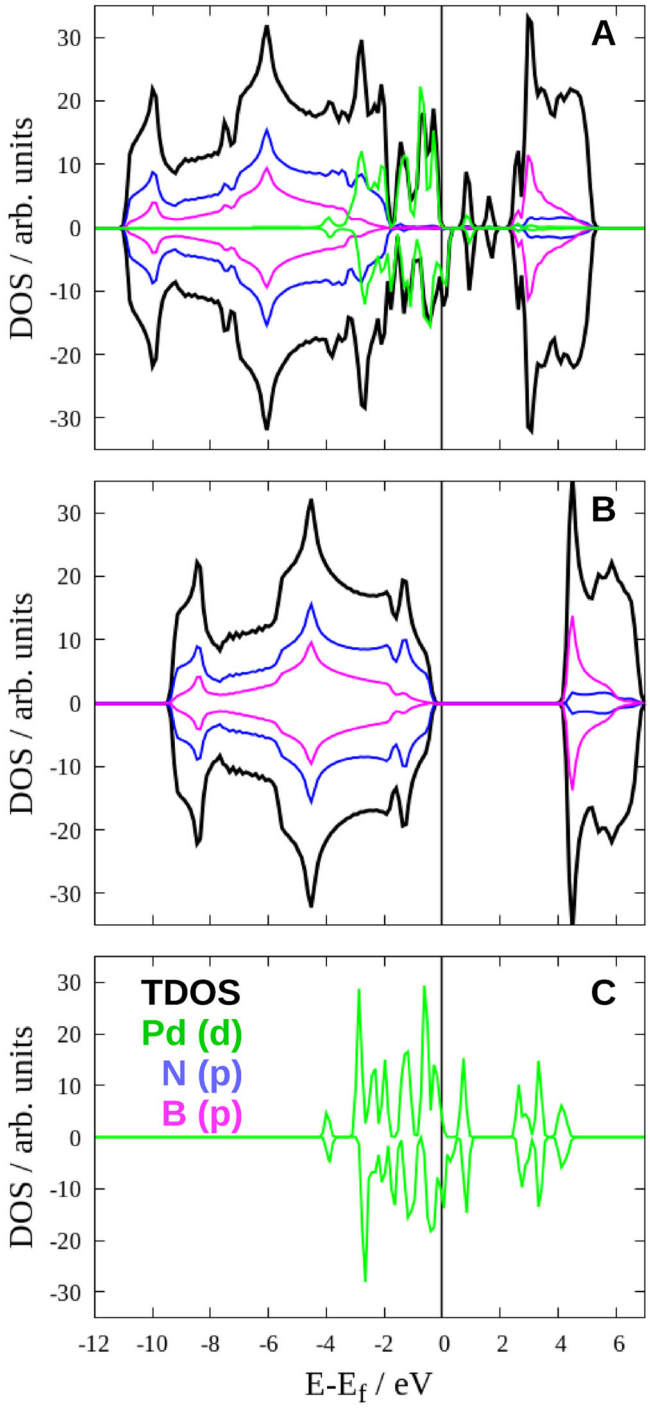


**Figure 2.** Projected density of states plot of A) *h*-BN supported $Pd_6$; B) *h*-BN sheet support; C) $Pd_6$ cluster optimized in vacuo. Total DOS (TDOS) obtained as the sum of each pDOS contribution are shown in black, Pd (4d) states in green, B (2p) states in pink, and N (2p) states in blue. The Fermi energy is taken as the zero of energy.

adsorption energies. We note that out of the six Pd atoms of the cluster, three are directly interacting with the nitrogen atoms of the support. Thus, it is reasonable that their properties may differ from the other three Pd atoms that are further away from the *h*-BN support. To account for this difference in proximities, adsorption and associated reactivity studies were performed on two different faces of the cluster, namely on the "top" and "lateral" faces. The "top" face is the triangular face whose properties should not be directly affected by the presence of the support, while the triangular "lateral" face is made up of two BN-interacting Pd atoms and a "top" atom, as shown in Figure 1.

For various metallic surfaces[26] it has been demonstrated that HCOOH can be found in two different adsorption modes: a perpendicular mode in which both the hydroxyl and carbonyl groups interact with the metal in a bidentate fashion (HCOOH*) and another in which HCOOH lies parallel to the surface (HCOOH$^f$). When HCOOH exhibits the perpendicular binding mode, the *trans* isomer has been found to be reactive, initiating HCOO–mediated decomposition, while in the case of parallel adsorption, the *cis* configuration has been found to be the precursor of the COOH–mediated dehydrogenation. The analogous HCOOH* and HCOOH$^f$ structures were optimized on the $Pd_6$ cluster, and they are reported in Figure 3. On the top face, the bidentate mode has an adsorption energy of $-82.4\ kJ\,mol^{-1}$ while the parallel mode has an adsorption energy of $-46.3\ kJ\,mol^{-1}$. These two results can be compared with those of Scaranto et al.,[3] which were obtained on a Pd(111) surface. For the same bidentate and parallel configurations they obtained adsorption energies of $-39.6$ and $-2.9\ kJ\,mol^{-1}$. Even taking into account the lack of dispersion interactions in the previous study, which are included here with Grimme-D3 semiempirical corrections, it is reasonable to infer that this large difference may be attributed to the higher reactivity of the cluster atoms, which are more undercoordinated compared to the Pd(111) surface atoms. We also studied other adsorption structures in which only the hydroxyl or the carbonyl group interacts with a Pd atom. While these are stable states, they bind 44.6 and 55.3 $kJ\,mol^{-1}$ less exothermically than HCOOH*. We found that the carbonyl group interacts with $Pd_6$ more strongly than the hydroxyl group.

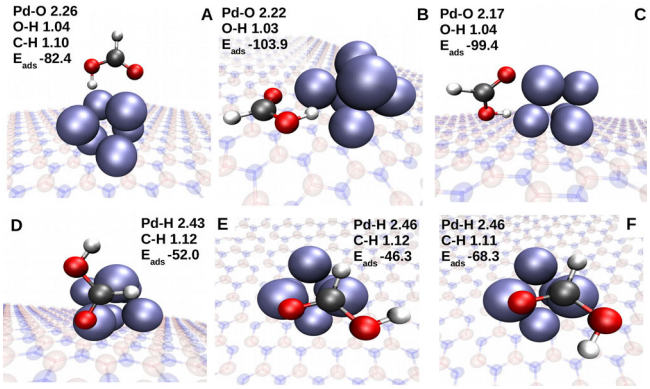


**Figure 3.** Optimized structures of HCOOH in its most stable adsorption modes: A) front view of the bidentate mode (HCOOH*) on the top face; B),C) side view of the bidentate mode (HCOOH*) on the lateral face, with opposite carbonyl/hydroxyl coordination; D) side view of parallel mode (HCOOH$^f$ ) on the lateral face; E) top view of the parallel mode (HCOOH$^f$) on the top face (*cis*); F) top view of the parallel mode (HCOOH$^f$) on the top face (*trans*). For each panel, relevant bond lengths (in Å) and adsorption energies ($E_{ads}$, in $kJ\,mol^{-1}$) are reported.


© 2017 Wiley-VCH Verlag GmbH & Co. KGaA, Weinheim

On the lateral side of the cluster, two stable bidentate binding modes were identified. The two HCOOH oxygens can interact with the Pd atoms of this face in two different ways: 1) the carbonyl can be adsorbed on the *N*-interacting Pd atoms while the hydroxyl interacts with the Pd atom belonging to the top face (Figure 3B); or 2) vice versa (Figure 3C). We found that the optimized structures arising from cases (1) and (2) are nearly isoenergetic with adsorption energies of −103.9 and −99.4 kJ mol$^{-1}$, respectively. We note here that HCOOH adsorbs more strongly on the lateral than the top face by approximately 20 kJ mol$^{-1}$. The *cis* HCOOH[f] on the lateral face (Figure 3D) instead adsorbs as strongly as on the top face, with an adsorption energy enhanced only by 5.7 kJ mol$^{-1}$. As a result, the perimetral sites of $Pd_6$, in direct contact with the support, should be the first to be occupied by HCOOH, and the top sites might be occupied subsequently.

### HCOOH decomposition

Metal-catalyzed formic acid decomposition has been studied extensively (Scheme 1).[3–6] To study the competition between

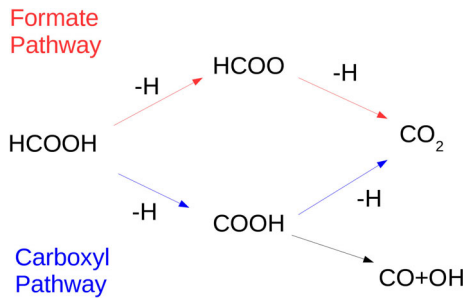


**Scheme 1.** Reaction scheme for formic acid decomposition.

HCOO and COOH–mediated paths, and also the different reactivity of top and perimetral sites of the cluster, the following procedure was used: 1) reaction intermediates and transition states (TS) associated with the first hydrogen abstraction in the HCOO and COOH–mediated paths were optimized on the top and on the lateral face of the cluster, following the convention illustrated in Figure 1; 2) the final state (FS) of the first molecular event was re-optimized varying the adsorption site of the lost hydrogen atom; 3) the most stable configuration found was then used as best initial state (BIS) for the abstraction of the second hydrogen atom.

### Top face: HCOO–mediated path

From the previously reported bidentate adsorption mode, HCOOH can decompose via HCOO, beginning with breaking of the O–H bond. On the top face of the cluster, this process requires an activation energy of 26.6 kJ mol$^{-1}$ and is exothermic by −41.0 kJ mol$^{-1}$ (see Figure 4).

At this point, a coordination change should occur to break the C–H bond, as the C–H bond of HCOO in the bidentate adsorption mode is too far away from the cluster to be activated.

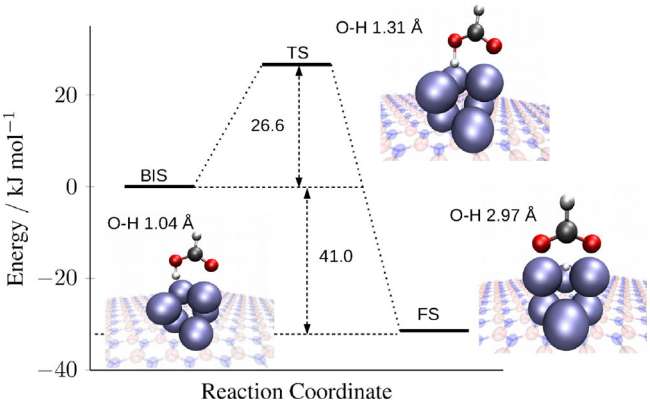


**Figure 4.** Energy profile for the HCOOH→HCOO+H step on the top face of the supported $Pd_6$ cluster. The optimized structures of best initial state (BIS), transition state (TS), and final state (FS) are shown in the insets, together with relevant geometric descriptors (breaking O–H bond length).

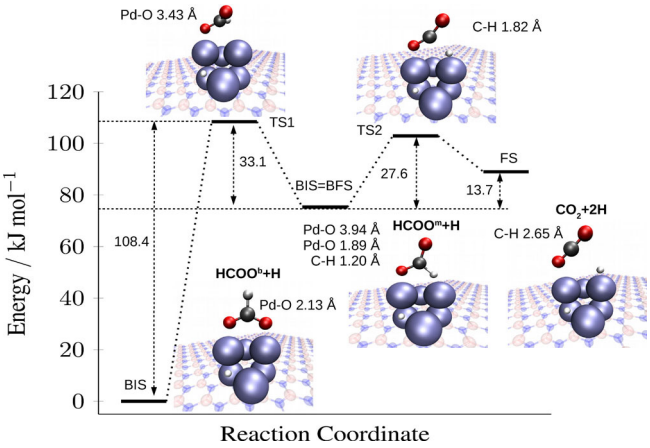


**Figure 5.** Energy profile for the HCOO→$CO_2$+H elementary step, (through a coordination change step: bidentate ($HCOO^b$) to monodentate ($HCOO^m$) formate followed by H abstraction to the final products) on the top face of the supported $Pd_6$ cluster. The optimized structures of best initial state (BIS), transition state (TS), and final state (FS) are reported in the insets, along with relevant geometric descriptors (breaking bond lengths).

As shown in Figure 5, this reaction step, which is common on metallic surfaces,[3,26–28] requires 108.4 kJ mol$^{-1}$. The HCOO monodentate mode, characterized by close proximity of the remaining hydrogen to a Pd atom (Pd–H distance 1.89 Å), is 75.3 kJ mol$^{-1}$ less stable than the bidentate mode. This difference can be ascribed to the breaking of a strong Pd–O bond. The subsequent C–H bond cleavage in the monodentate HCOO requires an activation energy of 27.6 kJ mol$^{-1}$ and is endothermic by 13.7 kJ mol$^{-1}$. The final state has the hydrogen atom interacting with a Pd atom in an atop position. The best final state (BFS), reported in Figure 6A, shows both H atoms adsorbed on the $Pd_6$ faces, while $CO_2$ is almost desorbed from the top face of the cluster, with Pd–O bond distances longer than 3.0 Å.


© 2017 Wiley-VCH Verlag GmbH & Co. KGaA, Weinheim

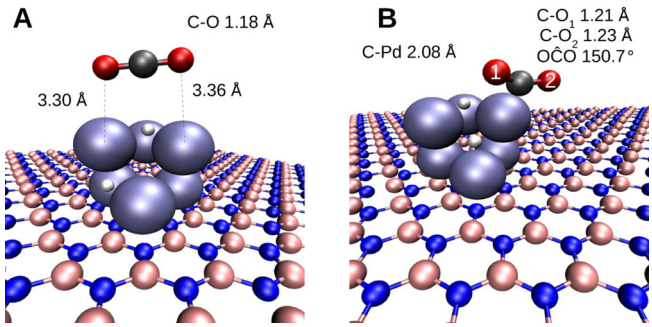


**Figure 6.** Optimized structure of $CO_2$ on the BN-supported $Pd_6$ cluster: A) linear geometry; B) bent (v-shape) geometry. Relevant geometrical parameters are reported.

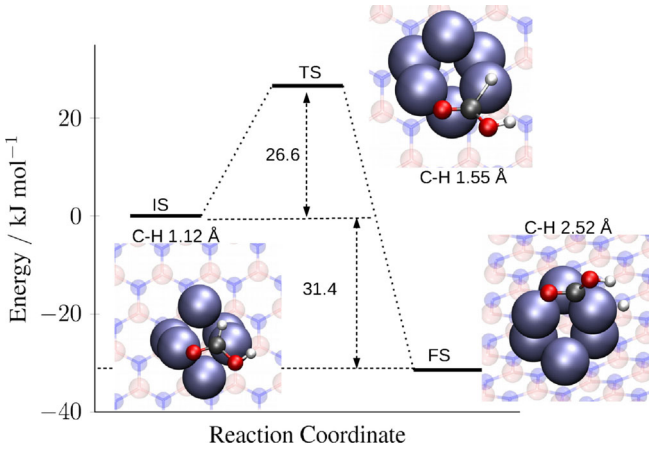


**Figure 7.** Energy profile for the HCOOH→COOH + H step on the top face of the supported $Pd_6$ cluster. The optimized structures of initial state (IS), transition state (TS), and final state (FS) are reported in the insets, along with relevant geometrical descriptors (breaking bond lengths).

### Top face: COOH path

Starting from the HCOOH[f] parallel adsorption mode, the carboxyl intermediate can be formed by breaking the C–H bond, which involves overcoming an activation energy of 26.6 kJ mol$^{-1}$ (see Figure 7). The hydrogen ends up atop of a Pd atom, with a bond distance of 1.59 Å, whereas the COOH interacts with the same Pd via its carbon atom, with a Pd–C bond distance of 1.95 Å. This particular configuration, which is similar to what was previously found on a Pd(111) surface,[3] allows for the interaction of the carbonylic oxygen with the Pd cluster; the Pd–O bond distance is 2.24 Å. All of these features contribute to an overall stabilization of the COOH + H co-adsorbed state by 31.4 kJ mol$^{-1}$ (see Figure 7) with respect to the initial state (IS).

In agreement with previous reports,[13,29] atop coordination of adsorbed hydrogen is not favored. In the optimized BIS, shown in Figure 8, the hydrogen atom has a threefold coordination. We also note that the carboxyl intermediate in this state is suitably positioned for the subsequent reaction step, since the hydroxyl moiety points directly toward one of the $Pd_6$ faces. The second dehydrogenation step, leading from

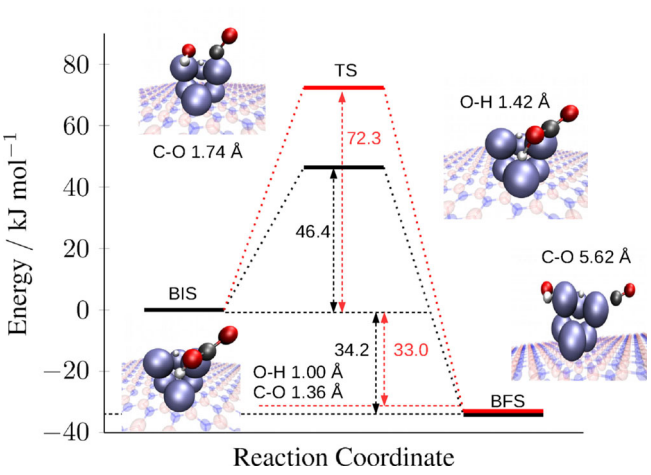


**Figure 8.** Energy profile for the COOH→$CO_2$ + H (black) and COOH→CO + OH (red) steps on the top face of the supported $Pd_6$ cluster. The optimized structures of best initial state (BIS), transition state (TS), and best final state (BFS) are reported in the insets, along with relevant geometrical descriptors (breaking-bond lengths).

COOH to $CO_2$, has an activation energy of 46.4 kJ mol$^{-1}$. This latter elementary step is exothermic by 34.2 kJ mol$^{-1}$ (see Figure 8). Interestingly, the adsorbed $CO_2$ product exhibits a bent geometry, as detailed in Figure 6 B. According to a previous report,[30] this particular geometry arises from negative charge transfer from the metal to the antibonding orbitals of $CO_2$. Indeed, Bader charge analysis performed in this case demonstrates a charge transfer of $-0.4|e|$ from the cluster to the adsorbed $CO_2$, in agreement with the study of Ko et al. performed on a Pd(111) extended surface.[30] The bent $CO_2$ geometry is also the preferred one on a reduced ceria support.[31] The stability of this structure with respect to the classical linear $CO_2$ geometry in fact depends on the metal: as examples on Ru(0001) the bent structure is more stable than the linear one, whereas on Pd(111) and Ni(111) physisorbed linear $CO_2$ is favored.[32] On $Pd_6$, we find that the bent structure is 53.8 kJ mol$^{-1}$ more stable than the linear one.

Finally, it should be mentioned that in the COOH path–mediated, complete dehydrogenation is not the only possible fate for the carboxyl intermediate; CO and OH can also be formed by breaking of the C–OH bond. We calculated that this step has an activation energy of 72.3 kJ mol$^{-1}$ (see Figure 8), circa 26 kJ mol$^{-1}$ more than the COO–H bond breaking step, indicating a strong selectivity preference towards $CO_2$ elimination, instead of CO production.

### Perimeter sites

One of the first effects that a support could exert on sub-nanometer sized clusters, before invoking more specific processes involving charge transfer or reconstruction, is the breaking of the symmetry that the sub-nanometer clusters possess when unsupported. While $Pd_6$ retains a nearly octahedral structure on BN, the Pd atoms interacting with the support may show different catalytic properties with respect to those belonging to the "top face" of $Pd_6$. The energy profile and optimized


© 2017 Wiley-VCH Verlag GmbH & Co. KGaA, Weinheim

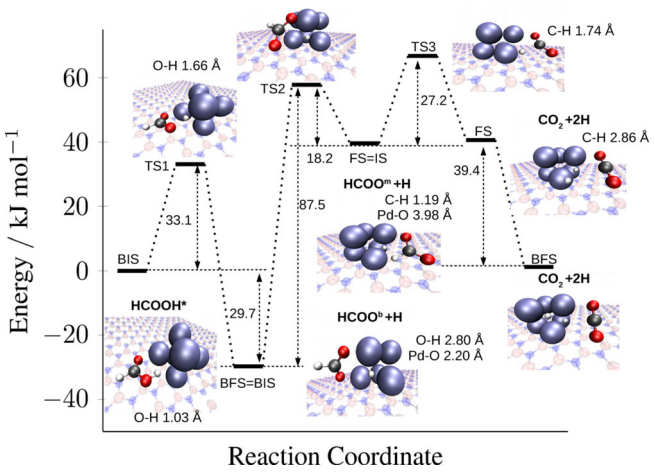


**Figure 9.** Energy profile for HCOOH decomposition through the HCOO–mediated path on the lateral side of the supported $Pd_6$ cluster. The optimized structures of (best) initial state ((B)IS), transition state (TS), and (best) final states ((B)FS) are reported in the insets, along with relevant geometric descriptors (breaking bonds lengths). $HCOO^m$ and $HCOO^b$ indicate the monodentate and bidentate formate, respectively.

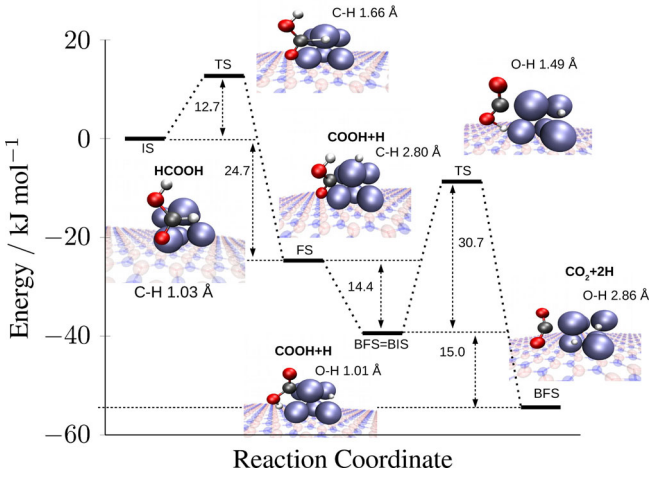


**Figure 10.** Energy profile for HCOOH decomposition through the COOH–mediated path on the lateral side of the supported $Pd_6$ cluster. The optimized structures of (best) initial state ((B)IS), transition state (TS), and (best) final states ((B)FS) are reported in the insets, along with relevant geometrical descriptors (breaking–bonds length).

structures of TSs and reaction intermediates related to the HCOO-mediated or COOH-mediated decomposition of HCOOH on the perimetral sites of the cluster are reported in Figure 9 and Figure 10, respectively.

Following the HCOO–mediated path, to produce HCOO from the initial adsorbed HCOOH, a barrier of 33.1 kJ mol$^{-1}$ has to be overcome. The reaction is exothermic by 29.7 kJ mol$^{-1}$ (see Figure 9). From this state, bidentate to monodentate HCOO conversion occurs with an activation energy of 87.5 kJ mol$^{-1}$; similarly to what was found on the top face, this step is endothermic: the monodentate state is 69.3 kJ mol$^{-1}$ higher in energy than the bidentate one. The final dehydrogenation step in this path requires an activation energy barrier of 27.2 kJ mol$^{-1}$.

Alternatively, HCOOH can dehydrogenate following the COOH–mediated path. The C–H bond cleavage step requires a very low activation energy barrier of 12.7 kJ mol$^{-1}$ (see Figure 10). Notably, this value is 13.9 kJ mol$^{-1}$ lower than that found on the top face of the cluster. This difference can be ascribed to the destabilization of the initial state, adsorbed HCOOH[f], with respect to that found on the top face. Both the hydrogen atom and the carboxyl fragment formed from the first dehydrogenation are atop-coordinated to the same Pd atom, with Pd–C and Pd–H bond lengths of 1.95 Å and 1.59 Å, respectively. In the BFS, a structural rearrangement of the carboxyl along with a change in the hydrogen coordination (from atop to threefold) results in an overall stabilization of 14.4 kJ mol$^{-1}$ with respect to the FS. In the BFS, unlike in the FS, the hydroxyl points toward the lateral side of the cluster and thus a further dehydrogenation step is conceivable. The final elementary step: $COOH + H \rightarrow CO_2 + 2H$ is exothermic by 15.0 kJ mol$^{-1}$, and has an activation energy of 30.7 kJ mol$^{-1}$. The $CO_2$ produced exhibits a bent geometry, while both the hydrogen atoms are coordinated to one of the triangular faces of $Pd_6$.

## Discussion

### Size sensitivity

It is interesting to compare the results presented herein with those of previous studies dealing with HCOOH decomposition on a Pd(111) surface. This comparison should allow us to evaluate how the sub-nanometer size of the cluster affects HCOOH decomposition reactivity. Furthermore, although nanoparticles often undergo sintering and coalescence during catalytic processes, the $Pd_6$ system could be informative for understanding the beginning stages of a catalytic system, before the catalyst particles agglomerate and their properties evolve toward

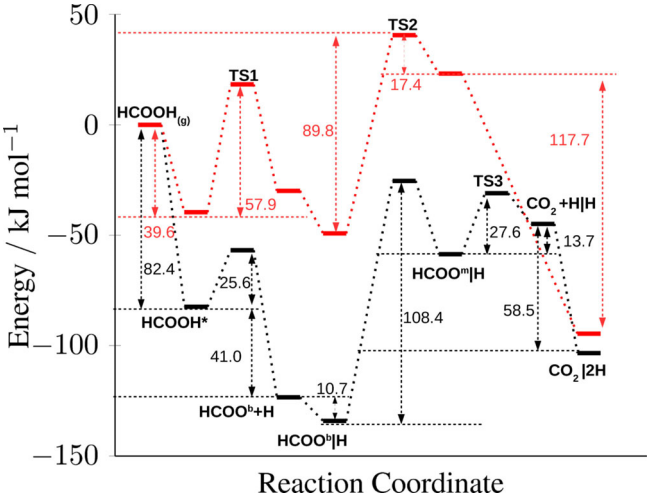


**Figure 11.** Energy profile for HCOOH decomposition, through the HCOO–mediated path on the top face of the *h*-BN supported $Pd_6$ cluster (black lines) and on a clean Pd(111) surface (red lines, adapted from Scaranto et al.[3]). The vertical bar notation (A|B) indicates, for the cluster, the most stable co-adsorbed configuration of A and B and for the Pd surface adsorption of A and B at infinite separation.


© 2017 Wiley-VCH Verlag GmbH & Co. KGaA, Weinheim

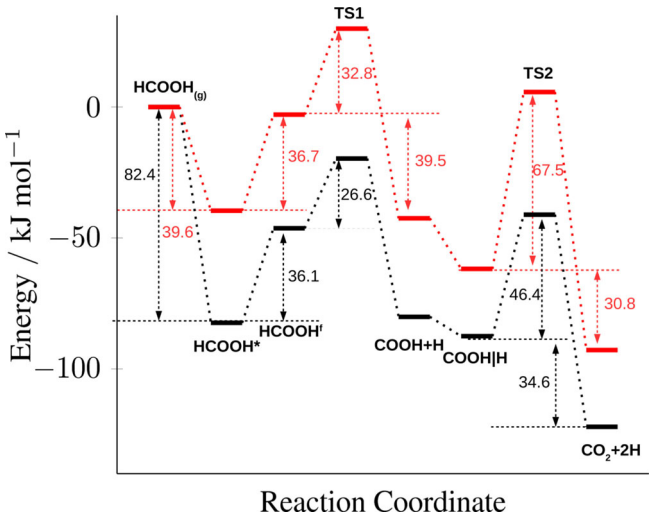


**Figure 12.** Energy profile for HCOOH decomposition, through the COOH–mediated path on the top face of the *h*-BN supported $Pd_6$ cluster (black lines) and on a clean Pd(111) surface (red lines, adapted from Scaranto et al.[3]). The vertical bar notation (A | B) indicates, for the cluster, the most stable co-adsorbed configuration of A and B, and for the Pd surface adsorption A and B, at infinite separation.

those of a more typical Pd nanoparticle. The energy profile of the HCOO-mediated path on the top face of the supported $Pd_6$ and on a Pd(111) surface (adapted from Scaranto et al.[3]) are shown in Figure 11, while the corresponding comparison for the COOH-mediated path is reported in Figure 12.

A first inspection of Figure 11 reveals the pronounced difference between the HCOO reaction path on the cluster and on the surface.

First, on $Pd_6$ the HCOO–mediated path is stabilized with respect to the Pd(111) surface, with differences in energy up to 50 kJ mol$^{-1}$ in the case of adsorbed HCOO. Second, the number of elementary steps in the reaction mechanism is different: on Pd one additional step. On Pd(111) it has been instead reported that once the formate converts from bidentate to the monodentate conformation, dehydrogenation leading to $CO_2$ is spontaneous, as opposed to the cluster, where another transition state needs to be crossed in order to dehydrogenate the monodentate HCOO.

In that respect, it should be noted that while on Pd(111) both TS1 and the monodentate HCOO are energetically well above the reference HCOOH gas phase, these two states are stabilized on the cluster and lie below the gas phase HCOOH. This is very likely due to a stronger interaction of these intermediates with the more undercoordinated metal atoms present on the cluster. For the same reason, some interesting differences arise also in the activation energies of selected steps: for example the energetic requirement for the first dehydrogenation is considerably lower on the cluster (25.6 vs. 57.9 kJ mol$^{-1}$). The activation energy for the bidentate to monodentate HCOO transformation is however 18.9 kJ mol$^{-1}$ higher on the cluster than on the Pd surface.

In the case of the COOH–mediated path, the differences between the (111) surface and the cluster are fewer, as shown in Figure 12. Apart from an overall stabilization of the reaction intermediates and transition states, for the same reasons as those discussed for the HCOO–mediated path, the reaction mechanism shows no significant differences, with the only exception of a higher activation barrier for the second dehydrogenation step on Pd(111) as compared to the cluster (67.5 vs. 46.4 kJ mol$^{-1}$). For the first dehydrogenation step the energetic requirement is nearly identical for the two cases, with a difference within 7 kJ mol$^{-1}$. This is due to the geometric features that TS1 shows both on the cluster and surface: in particular the C–H bond lies almost exactly on a single metal atom, in an $\eta^2$ coordination between C, H, and Pd. Interestingly, the same TS coordination mode has been recently found by He and Hua Li,[33] who studied, with a variety of exchange-correlation functionals, a monoatomic Pd catalyst for HCOOH decomposition. According to their results, the above–mentioned TS structure is the one associated with the lowest activation energy barrier for the COOH path.

### Competition between HCOO- and COOH-mediated paths

The energy profiles for HCOOH dehydrogenation through the two selected paths are displayed in Figure 13. Both reflected reactivity at the top face. For the sake of clarity, reactivity of the perimeter sites will be discussed subsequently. A simple analysis suggests that decomposition through the HCOO–mediated path could take place. Indeed, although the energetic requirement for the first HCOOH dehydrogenation is approximately the same in both paths, in order to react through a COOHl-mediated mechanism, HCOOH would require a change in its adsorption mode from the most stable perpendicular conformation to the metastable nearly parallel HCOOH$^f$ conformation. Moreover, it is worth noting the large stabilization of the HCOO + H co-adsorbed state with respect to the COOH + H one.

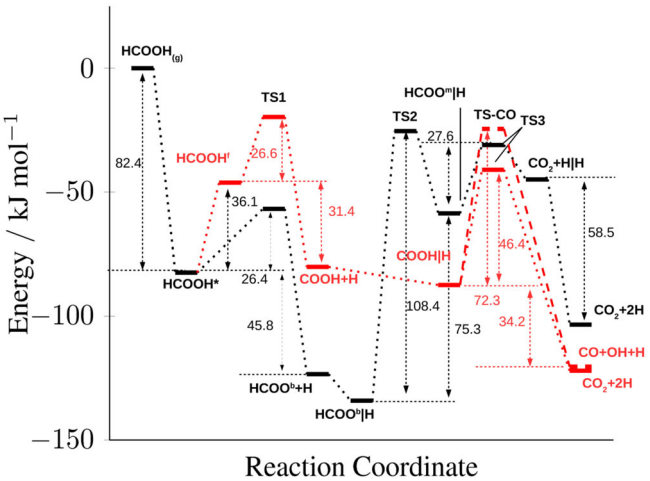


**Figure 13.** Energy profile for HCOOH decomposition, through the HCOO- (black lines) and COOH–mediated (red lines) pathways, on the top face of the *h*-BN supported $Pd_6$ cluster; the dashed red line is associated with breaking of C–OH of COOH, leading to CO + OH; the vertical bar notation (A | B) indicates the most stable co-adsorbed configuration of A and B on the cluster. $HCOO^m$ and $HCOO^b$ indicate monodentate and bidentate formate, respectively.


© 2017 Wiley-VCH Verlag GmbH & Co. KGaA, Weinheim

This is a rather unexpected result since, to the best of our knowledge, the large majority of the literature concerning HCOOH decomposition on Pd or Pt surfaces, reports stabilization of COOH with respect to HCOO.[3,26] This energetic difference of 37.1 kJ mol$^{-1}$ in the BFSs of HCOO + H versus COOH + H corroborates the hypothesis of a HCOO–mediated decomposition. Interestingly, Choi et al. have reported that relative stabilization of HCOO against COOH is structure-sensitive: COOH is more stable than HCOO both on Pd(111) and Pd(100) but the difference tends to zero on a (211) stepped surface.[34] Independently, Ju Li et al., have also found that on an unsupported $Pd_7$ cluster, HCOO is more stable than COOH.[35] These findings, together with our calculations, suggest that the preferential stabilization of HCOO against COOH could be affected by undercoordinated metal sites. In fact, a similar trend has been found in the case of alumina supported sub-nanometer $Cu_4$ clusters.[36]

This stabilization of HCOO over COOH could be a key factor for indirectly avoiding CO poisoning, since the high thermodynamic stability of HCOO should prevent the reaction flux from passing through the COOH intermediate, which is generally more reactive toward CO–OH bond breaking. However, on our supported $Pd_6$ cluster, even if HCOOH underwent COOH–mediated decomposition, the activation barrier for breaking the CO–OH bond in COOH is 25.9 kJ mol$^{-1}$ higher than that associated with its dehydrogenation, that is, the COO–H bond cleavage. CO poisoning thus should not be a major issue on *h*BN-supported $Pd_6$ clusters. However, the high energy requirement for HCOO reorientation as well its high degree of stabilization suggests possible HCOO poisoning of the supported $Pd_6$ cluster.

A complete picture of the catalyst activity and selectivity toward the formation of $CO_2$ cannot be estimated without taking into account the reactivity of the perimetral sites too. Figure 14 shows the energy profile for the HCOO-mediated and COOH-mediated decomposition paths on the side of the cluster. The conclusions regarding the reaction mechanism as well as the energetics are similar to those already discussed for the top face reactivity. While some differences can be observed, it is difficult to assess how significantly this can affect the overall reactivity. It is evident that there is a significant decrease of the activation barrier required for the bidentate HCOO to change its coordination mode, going from 108.4 kJ mol$^{-1}$ found on the top face to the more affordable value of 87.5 kJ mol$^{-1}$ on the side of the cluster. A decrease of a similar magnitude can also be found both for the first and second dehydrogenation steps of the COOH–mediated path. For the first dehydrogenation, a stabilization of TS1 and in the second a destabilization of the carboxyl initial state contributes to lowering of the activation barriers compared to those on the top face. Together with the stabilization of TS2 these numbers suggest weaker interaction of intermediates with the side of the metallic cluster, which may be ascribed to the effect of the support-Pd atoms interacting with the *h*-BN being more coordinated than the top face Pd atoms. This likely affects both the energy required to break the Pd–O bond (for example, TS2) and the stability of adsorbed intermediates (for example, COOH). Similar correlations relating the coordination of Pd atoms and to catalytic activity have been also discussed by Fampiou and Ramasubramaniam for a defective graphene-supported $Pt_{13}$ cluster.[37]

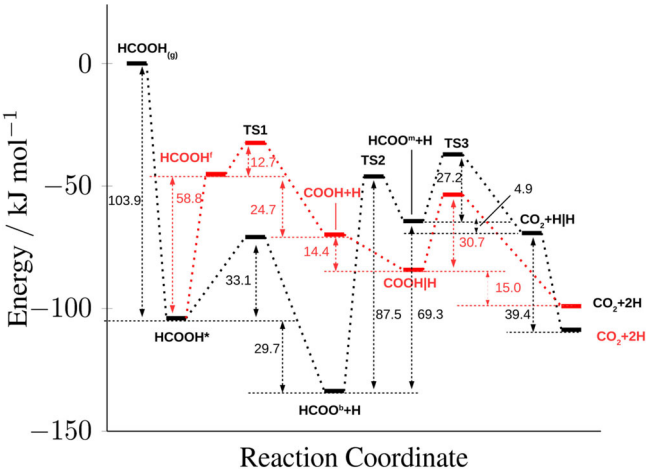


**Figure 14.** Energy profile for HCOOH decomposition, through the HCOO (black lines) and COOH mediated (red lines) paths, on the lateral side of the *h*-BN supported $Pd_6$ cluster. The vertical bar notation (A | B) indicates the most stable co-adsorbed configuration of A and B on the cluster. $HCOO^m$ and $HCOO^b$ indicate monodentate and bidentate formate, respectively.

### Hydrogen spillover

Finally, we will briefly discuss how hydrogen could diffuse on the various parts of the system studied. In particular, owing to the high stability of HCOO, it is interesting to explore the possible influence of co-adsorbed HCOO (top face coordinated) on the diffusion of an H atom on the cluster or onto the support.

Irrespective of the presence of HCOO, all trial structures in which a hydrogen atom is placed on an N or B atom in the proximity of the cluster converge after full optimization into structures in which the hydrogen interacts with $Pd_6$. In particular, H shows the threefold coordination on the cluster face nearest to the support. Optimizing H on a N or B atom further away from the cluster (approximately 6.0 Å away from the Pd–N anchoring point), we obtained two structures characterized by atop N and B coordination, with bond distances of 1.04 and 1.37 Å, respectively. Thus, it is reasonable to conclude that hydrogen prefers to interact with the Pd cluster, at least at these specific coverage conditions. Similarly, Yakobson and co-workers[38] have shown that for a graphene supported $Pd_4$ cluster H spillover onto the support is thermodynamically unfavorable at low hydrogen coverages. The energy profile for H diffusion on the supported cluster faces, via the connecting edges, in the presence or absence of co-adsorbed HCOO, are reported in Figure 15 and Figure 16, respectively.

The hydrogen adsorption energy on the supported $Pd_6$ cluster is 53.7 kJ mol$^{-1}$ in the presence of HCOO, while it is slightly lower (49.8 kJ mol$^{-1}$) on the clean cluster. For comparison, Santana and Rösch found an adsorption energy of 70 kJ mol$^{-1}$ for H in the case of a gold supported $Pd_3$ sub-nanometric cluster.[39] The diffusion barriers are generally higher on the clean


© 2017 Wiley-VCH Verlag GmbH & Co. KGaA, Weinheim

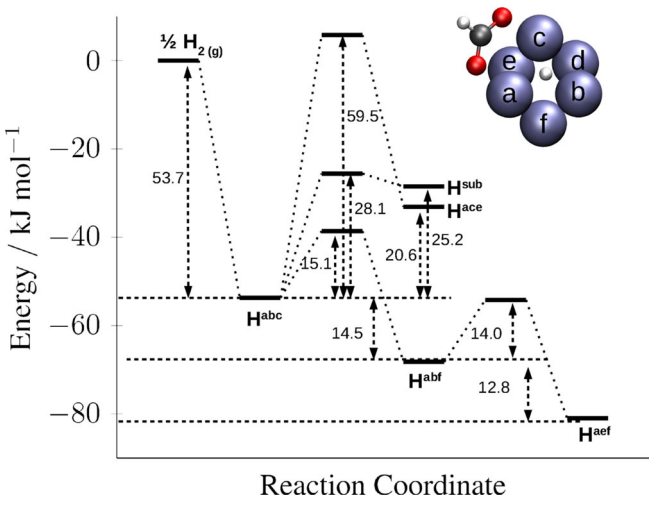


**Figure 15.** Energy profile for hydrogen diffusion via different faces of the *h*-BN supported $Pd_6$ cluster, in the presence of a co-adsorbed HCOO species. The inset shows the optimized structure of HCOO and H, coordinated to the $Pd_6$ *abc* face (the *h*-BN layer was omitted for clarity, Pd(f), Pd(e), and Pd(d) interact with the support, via N atoms). The superscripts indicate the cluster face to which hydrogen is coordinated, according to the convention highlighted in the inset; the superscript "sub" indicates that hydrogen is coordinated to the center of the cluster.

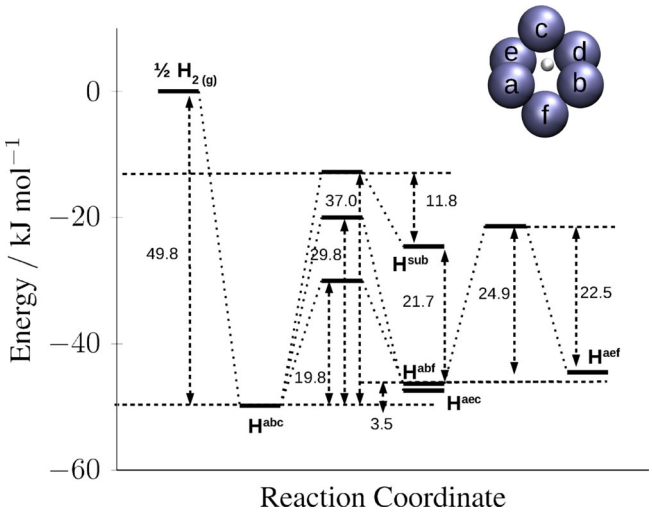


**Figure 16.** Energy profile for hydrogen diffusion via different faces of the *h*-BN supported $Pd_6$ cluster. The inset shows the optimized structure of H, coordinated to the *abc* face (the *h*-BN layer was omitted for clarity, Pd(f), Pd(e), and Pd(d) interact with the support, via N atoms). The superscripts indicate the cluster face to which hydrogen is coordinated, according to the convention highlighted in the inset; the superscript "sub" indicates that hydrogen is coordinated to the center of the cluster.

cluster than when HCOO is co-adsorbed, suggesting a repulsive interaction between the two adsorbates. On the HCOO-covered supported $Pd_6$ cluster, diffusion barriers in the range between 14.1–59.5 kJ mol$^{-1}$ were calculated. The highest barrier is associated with diffusion from the *abc* (top) to the *ace* face (see Figure 15). It can be seen that all diffusion barriers are much lower than the energy required for the HCOO reorientation necessary for HCOO decomposition; thus, diffusion should not have a significant influence on the overall reaction mechanism.

On the naked supported cluster (see Figure 16), the adsorption of H on all the investigated threefold sites resulted isoenergetic (within 4 kJ mol$^{-1}$). Instead, on the HCOO–covered cluster the hydrogen atom prefers to adsorb on the *aef* face.

Diffusion from the *abc* (top) face to the center of the cluster was also investigated. Although this is not well-studied in the literature in the case of sub-nanometer clusters, this mechanism could be reminiscent of the common subsurface hydrogen migration mechanisms, well studied in the case of palladium catalysts. Both on the clean and HCOO–covered clusters, this particular hydrogen state ($H^{sub}$) is thermodynamically unfavored. Diffusion from the *abc* (top) face is endothermic by 25.2 kJ mol$^{-1}$, while the activation barriers for the diffusion are 37.0 kJ mol$^{-1}$ on the clean cluster and 28.1 kJ mol$^{-1}$ on the HCOO–covered cluster.

## Conclusions

A detailed DFT study of formic acid decomposition on a boron nitride supported $Pd_6$ sub-nanometer cluster was presented. The competition between the formate, HCOO-mediated, and the carboxyl, COOH-mediated dehydrogenation paths, occurring on the "top" and "lateral" faces of the metallic cluster was investigated.

On both types of reactive sites considered, the formic acid decomposition mechanism preferentially occurs through the HCOO-mediated path, as the HCOO intermediate is energetically much more stable than COOH. The formation of $CO_2$ from COOH was also demonstrated to be more favorable than CO production occurring through CO–OH bond breaking in COOH.

On the top face of the supported cluster, the highest activation barrier found, circa 108 kJ mol$^{-1}$, is associated with the conversion of HCOO from a bidentate to a monodentate HCOO. This is a candidate for the rate-determining step. The same elementary step has a lower energetic requirement on the lateral side of the cluster (87.5 kJ mol$^{-1}$) likely due to the coordination of the Pd atoms of this reaction site with the support, leading to a weaker Pd–O bond that needs to be broken in this step.

We compared the reactivity of the top face of the Pd cluster with state-of-the-art calculations on Pd extended surfaces and elucidated the role of undercoordinated sites, including how they control the reactivity of the sub-nanometer $Pd_6$ cluster. In particular, almost all barriers, for both HCOO- and COOH-mediated paths, are lower on the cluster than on the extended surface. The only exception is for the conversion of bidentate HCOO to monodentate HCOO, which is probably due to a stronger Pd–O interaction on $Pd_6$.

We also studied hydrogen spillover mechanisms to understand the energetics of diffusion on $Pd_6$ and on the support. We conclude that, at the early stages of the reaction (low coverage limit), migration toward the support is energetically unfavorable. Instead the diffusion between different threefold sites of the cluster can occur with lower activation energy bar-


© 2017 Wiley-VCH Verlag GmbH & Co. KGaA, Weinheim

riers. These barriers are slightly decreased in the presence of a co-adsorbed HCOO species.

## Computational Methods

All calculations were performed using the Vienna Ab initio Simulation Package (VASP).[40,41] Projector augmented wave (PAW) potentials were used to describe the core electron interactions, while a plane wave basis set with a kinetic energy cutoff of 500 eV was chosen to expand the electronic wave function of the valence electrons. The generalized gradient approximation (GGA) using the Perdew, Burke, and Ernzerhof (PBE)[42] exchange-correlation functional, including the Grimme-D3[43] semiempirical dispersion correction, was used. To simulate a *h*-BN monolayer, a $B_{48}N_{48}$ supercell was replicated in the xy plane, with 15.03 and 17.34 Å lattice constants. To avoid spurious interactions between the periodic images, a vacuum layer of at least 15 Å was used in the *z* direction. Owing to the relatively large supercell size, the sampling of the reciprocal space was restricted to the Γ-point. Spin-polarized calculations were carried out and all the structures were fully relaxed until the forces acting on the atoms were smaller than 0.02 eV Å$^{-1}$. All of the atoms were allowed to relax during optimization. This computational setup was tested through benchmarking calculations, ensuring the convergence of total energy with respect to both the energy cutoff and k-point sampling. Transition states (TS) were identified with the climbing image nudged elastic band method (CI-NEB)[44] using seven images in addition to the initial and final states. A convergence criterion of 0.1 eV Å$^{-1}$ was used for the forces, and the nature of the stationary point on the potential energy surface was checked by the calculation and inspection of vibrational frequencies. The growth pattern of sub-nanometer Pd clusters on BN supports was extensively studied in a previous study by Schimmenti et al.;[21] in agreement with this previous study, $Pd_6$ if supported onto a boron nitride nanotube (BNNT) exists in an octahedral geometry, which is the most stable among the $Pd_6$ geometric isomers. It was also demonstrated that the BNNT curvature has a negligible influence on the growth mechanism, implicitly suggesting here that the same octahedral $Pd_6$ structure can be used as a starting point for the *h*-BN supported cluster geometry optimization.

The adsorption energy ($E_{ads}$) of the Pd cluster on the *h*-BN was calculated as in Equation (1):

$$E_{ads} = E_{TOT} - E_{h\text{-}BN} - E_{Pd6} \quad (1)$$

where $E_{TOT}$ is the total energy of the system, $E_{h\text{-}BN}$ is the energy of the pristine boron nitride sheet supporting the $Pd_6$ cluster, and $E_{Pd6}$ is the energy of the gas-phase $Pd_6$ cluster. Using a similar expression, but taking the gas-phase energy of HCOOH as reference and substituting the second term of Equation (1) with the energy of the *h*-BN supported $Pd_6$, the adsorption energy of formic acid was calculated. The computational protocol chosen was able to correctly reproduce the most stable spin configuration of the isolated $Pd_6$, which as previously demonstrated,[21] is the triplet state. Adsorbates–cluster interactions did not lead to any significant $Pd_6$ geometrical changes. Test calculations were performed to evaluate the reactivity of the free, un-supported cluster, considering the HCOO decomposition pathway; negligible differences, within 10 kJ mol$^{-1}$, were found, suggesting that support effects may be insignificant for this case.

## Acknowledgements

*This work was partially supported by Department of Energy (DOE)-Basic Energy Sciences (BES), Division of Chemical Sciences (DE-FG02-05ER15731). The computational work was performed partially using supercomputing resources at National Energy Research Scientific Computing Center (NERSC). NERSC is supported by the U.S. Department of Energy, Office of Science, under contract DE-AC02-05CH11231. This research was also partially performed using the computing resources and assistance of the UW-Madison Center for High Throughput Computing (CHTC) in the Department of Computer Sciences. The CHTC is supported by UW-Madison, the Advanced Computing Initiative, the Wisconsin Alumni Research Foundation, the Wisconsin Institutes for Discovery, and the National Science Foundation. We thank Benjamin Chen and Ellen Murray for careful reading of the manuscript.*

**Keywords:** boron nitride · DFT · formic acid · palladium · sub-nanometer clusters

[1] J. Q. Bond, D. M. Alonso, D. Wang, R. M. West, J. A. Dumesic, *Science* **2010**, *327*, 1110 – 1114.
[2] A. Kirilin, A. Tokarev, E. Murzina, L. Kustov, J.-P. Mikkola, D. Yu Murzin, *ChemSusChem* **2010**, *3*, 708 – 718.
[3] J. Scaranto, M. Mavrikakis, *Surf. Sci.* **2016**, *650*, 111 – 120.
[4] S. Singh, S. Li, R. Carrasquillo-Flores, A. C. Alba-Rubio, J. A. Dumesic, M. Mavrikakis, *AIChE J.* **2014**, *60*, 1303 – 1319.
[5] Y.-X. Chen, M. Heinen, Z. Jusys, R. J. Behm, *ChemPhysChem* **2007**, *8*, 380 – 385.
[6] J. A. Herron, J. Scaranto, P. Ferrin, S. Li, M. Mavrikakis, *ACS Catal.* **2014**, *4*, 4434 – 4445.
[7] J. B. Benziger, R. J. Madix, *Surf. Sci.* **1979**, *79*, 394 – 412.
[8] Y.-K. Sun, W. H. Weinberg, *J. Chem. Phys.* **1991**, *94*, 4587 – 4599.
[9] S. W. Jorgensen, R. J. Madix, *J. Am. Chem. Soc.* **1988**, *110*, 397 – 400.
[10] J. L. Davis, M. A. Barteau, *Surf. Sci.* **1991**, *256*, 50 – 66.
[11] J. B. Benziqer, G. R. Schoofs, *J. Phys. Chem.* **1984**, *88*, 4439 – 4444.
[12] S. Vajda, M. G. White, *ACS Catal.* **2015**, *5*, 7152 – 7176.
[13] V. D'Anna, D. Duca, F. Ferrante, G. L. Manna, *Phys. Chem. Chem. Phys.* **2009**, *11*, 4077 – 4083.
[14] M. Becton, X. Wang, *Phys. Chem. Chem. Phys.* **2015**, *17*, 21894 – 21901.
[15] R. T. Paine, C. K. Narula, *Chem. Rev.* **1990**, *90*, 73 – 91.
[16] N. Sakhavand, R. Shahsavari, *J. Phys. Chem. C* **2014**, *118*, 22730 – 22738.
[17] Q. Weng, X. Wang, C. Zhi, Y. Bando, D. Golberg, *ACS Nano* **2013**, *7*, 1558 – 1565.
[18] J. Li, J. Lin, X. Xu, X. Zhang, Y. Xue, J. Mi, Z. Mo, Y. Fan, L. Hu, X. Yang, *Nanotechnology* **2013**, *24*, 155603 – 155610.
[19] N. Meyer, D. Pirson, M. Devillers, S. Hermans, *Appl. Catal. A* **2013**, *467*, 463 – 473.
[20] L. Gao, Q. Fu, M. Wei, Y. Zhu, Q. Liu, E. Crumlin, Z. Liu, X. Bao, *ACS Catal.* **2016**, *6*, 6814 – 6822.
[21] R. Schimmenti, R. Cortese, F. Ferrante, A. Prestianni, D. Duca, *Phys. Chem. Chem. Phys.* **2016**, *18*, 1750 – 1757.
[22] C.-A. Lin, J. C. Wu, J.-W. Pan, C.-T. Yeh, *J. Catal.* **2002**, *210*, 39 – 45.
[23] K. A. Kacprzak, I. Czekaj, J. Mantzaras, *Phys. Chem. Chem. Phys.* **2012**, *14*, 10243 – 10247.
[24] D. Duca, F. Ferrante, G. La Manna, *J. Phys. Chem. C* **2007**, *111*, 5402 – 5408.
[25] A. Prestianni, R. Cortese, F. Ferrante, R. Schimmenti, D. Duca, S. Hermans, D. Yu Murzin, *Top. Catal.* **2016**, *59*, 1178 – 1184.
[26] J. Scaranto, M. Mavrikakis, *Surf. Sci.* **2016**, *648*, 201 – 211.
[27] S. Li, J. Scaranto, M. Mavrikakis, *Top. Catal.* **2016**, *59*, 1580 – 1588.
[28] J. S. Yoo, F. Abild-Pedersen, J. K. Nørskov, F. Studt, *ACS Catal.* **2014**, *4*, 1226 – 1233.
[29] A. Granja, J. A. Alonso, I. Cabria, M. J. Lopez, *RSC Adv.* **2015**, *5*, 47945 – 47953.


© 2017 Wiley-VCH Verlag GmbH & Co. KGaA, Weinheim

[30] J. Ko, B.-K. Kim, J. W. Han, *J. Phys. Chem. C* **2016**, *120*, 3438 – 3447.
[31] Z. Cheng, C. S. Lo, *Phys. Chem. Chem. Phys.* **2016**, *18*, 7987 – 7996.
[32] G. Peng, S. J. Sibener, G. C. Schatz, S. T. Ceyer, M. Mavrikakis, *J. Phys. Chem. C* **2012**, *116*, 3001 – 3006.
[33] N. He, Z. H. Li, *Phys. Chem. Chem. Phys.* **2016**, *18*, 10005 – 10017.
[34] S.-I. Choi, J. A. Herron, J. Scaranto, H. Huang, Y. Wang, X. Xia, T. Lv, J. Park, H. Peng, M. Mavrikakis, Y. Xia, *ChemCatChem* **2015**, *7*, 2077 – 2084.
[35] S. J. Li, X. Zhou, W. Q. Tian, *J. Phys. Chem. A* **2012**, *116*, 11745 – 11752.
[36] C. Liu, B. Yang, E. Tyo, S. Seifert, J. DeBartolo, B. von Issendorff, P. Zapol, S. Vajda, L. A. Curtiss, *J. Am. Chem. Soc.* **2015**, *137*, 8676 – 8679.
[37] I. Fampiou, A. Ramasubramaniam, *J. Phys. Chem. C* **2012**, *116*, 6543 – 6555.
[38] A. K. Singh, M. A. Ribas, B. I. H. Yakobson, *ACS Nano* **2009**, *3*, 1657 – 1662.
[39] J. A. Santana, N. Rösch, *Phys. Chem. Chem. Phys.* **2012**, *14*, 16062 – 16069.
[40] G. Kresse, J. Furthmuller, *Comput. Mater. Sci.* **1996**, *6*, 15 – 50.
[41] G. Kresse, J. Furthmuller, *Phys. Rev. B* **1996**, *54*, 11169 – 11186.
[42] J. P. Perdew, K. Burke, M. Ernzerhof, *Phys. Rev. Lett.* **1996**, *77*, 3865 – 3868.
[43] S. Grimme, J. Antony, S. Ehrlich, H. Krieg, *J. Chem. Phys.* **2010**, *132*, 154104 – 154110.
[44] G. Henkelman, B. P. Uberuaga, H. Johnson, *J. Chem. Phys.* **2000**, *113*, 9901 – 9904.

Manuscript received: February 6, 2017
Accepted Article published: ■■ ▮▮, 0000
Final Article published: ■■ ▮▮, 0000


© 2017 Wiley-VCH Verlag GmbH & Co. KGaA, Weinheim

*R. Schimmenti, R. Cortese, D. Duca,* M. Mavrikakis**

■■ – ■■

**Boron Nitride-supported Sub-nanometer $Pd_6$ Clusters for Formic Acid Decomposition: A DFT Study**

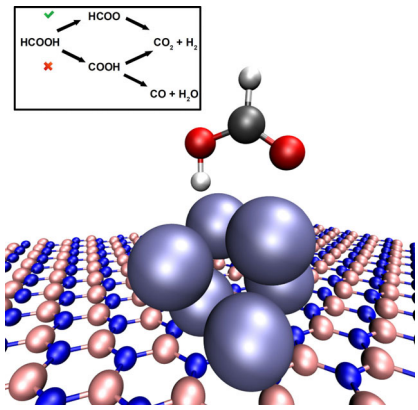


**Sub-nano key:** Density functional theory calculations offer atomistic insights into the catalytic activity of a $Pd_6$ sub-nanometer cluster, supported on a boron nitride sheet, for formic acid decomposition. Undercoordination of the cluster sites may be a key factor for avoiding CO production and poisoning.


© 2017 Wiley-VCH Verlag GmbH & Co. KGaA, Weinheim